

We are IntechOpen, the world's leading publisher of Open Access books Built by scientists, for scientists

6,900

Open access books available

186,000

International authors and editors

200M

Downloads

Our authors are among the

154

Countries delivered to

TOP 1%

most cited scientists

12.2%

Contributors from top 500 universities



WEB OF SCIENCE™

Selection of our books indexed in the Book Citation Index
in Web of Science™ Core Collection (BKCI)

Interested in publishing with us?
Contact book.department@intechopen.com

Numbers displayed above are based on latest data collected.

For more information visit www.intechopen.com



Design, Construction and Validation of a High-Performance OATS

Donglin Meng

Abstract

The state of the art on the open-area test site (OATS) has been introduced. Key technologies on the design and validation of a high-performance OATS have been provided. Some famous OATS in the world regarding their structure, the dimensions of the ground plane (GP), the location of the control room, and performance are listed in a table. A case study is provided on NIM's high-performance OATS. Many details are open for the first time, which show the fine design. A measurement uncertainty example has been provided in measuring the free-space antenna factor of biconical antennas. These results are based on the author's many years of experience, with lots of valuable data and photos. It is intended for calibration laboratories, for EMC antenna users, for writing EMC standards, as well as for the assessors in EMC.

Keywords: antenna factor, antenna calibration, open-area test site, calculable dipole antennas, site validation, site insertion loss

1. Introduction

An open-area test site (OATS) is one of the key facilities in EMC. An OATS is a basic facility to measure the antenna factor [1] and the “benchmark” for semi-anechoic chambers over (30–1000) MHz [2].

When we make radiated disturbance measurements, both antennas and anechoic chambers are required. An OATS is the best choice for measuring the antenna factor over 30 MHz to 1000 MHz. We use antennas to “capture” the invisible electric fields (E-fields) or magnetic fields (M-fields) by converting the fields into voltage signals, which can be measured by an EMI receiver. However, the converting capabilities are different for different antennas. Thus, we need a parameter to “eliminate” this difference; thus, the antenna factor is defined as the ratio between the magnitude of E-field and the voltage induced on the load (usually 50 Ω) connected into the feed of an antenna [1]. One of the major activities for a calibration laboratory is to measure their value. In order to get a very accurate value for the antenna factor over 30 to 1000 MHz, OATS is the best choice since it can provide the most accurate value for broadband EMC antennas over this frequency band.

An OATS is the “benchmark” for semi-anechoic chambers over (30–1000) MHz. An EMC chamber can isolate the radiated emission by an EUT from others by

a shielding enclosure outside the antenna and EUT. Usually, absorbers are lined inside to reduce the reflections along the four sides of an EUT and from the ceiling. However, it is very difficult to reduce totally due to the limits of technology and cost. Therefore, a quality verification process called validation is needed. The basic idea of this validation procedure is to measure the site attenuation (SA) between a pair of broadband antennas in the EMC chamber over (30–1000) MHz and compared with some standard value, which is defined as antenna pair reference site attenuation, A_{apr} [3]. If the difference is less than some value (e.g., 4 dB or less), then the EMC chamber can be regarded as a qualified “compatible test site” (COMTS). Thus the accuracy of A_{apr} is significant for the suppliers and end-users of the EMC chamber. Up to now, the OATS is the only way to measure the A_{apr} accurately. “Normalized site attenuation” (NSA) can be used to validate the performance of EMC chambers [3], too; however, OATS is also required to measure the free-space antenna factor and the mutual coupling, etc., are very difficult to get [4, 5].

Due to the significance of OATS in the EMC area, it is worthwhile reviewing the technologies of design, construction and validation of a high-performance OATS for the following:

- the antenna users
- calibration Labs
- potential builders of high-performance OATS
- certificate examiners
- revisions of international standards CISPR 16–1-6, CISPR 16–1-5, ANSI C63.5, and so on.

The start of the art on the OATS is introduced in Section 2; a detailed case study is provided on the design, construction, and validation in Section 3. An uncertainty example in measuring A_{apr} is provided in Section 4.

2. The state of the art on OATS in the world

The theoretical model of an OATS is listed in **Figure 1**. The electromagnetic fields (EM fields) radiated by a transmit antenna (Tx) are reflected only by the ground plane (GP), and the GP is infinitely large, consisting of a perfect electric conductor. Then, there are no other reflections. The receive antenna (Rx) received the EM fields radiated directly from the Tx and the reflections from the ground plane. Any other reflections are regarded as uncertainty sources. This means the better the ground plane size, the better agreement with an ideal OATS. Standard CISPR 16–1-5 states the minimum should be 30 m by 20 m. The most common ground plane size is 60 m by 30 m. The flatness of the metal ground plane is also important, especially above 700 MHz [6].

There are basically two types of structures on the large ground plane, as shown in **Figure 2**. In the solid type, the metal ground plane is placed directly on the surface of the concrete layer. This structure makes sure the metal ground plane can hold heavy EUT. In order to adjust the flatness of the ground plane, some space is designed between the metal ground plane and the concrete layer, which is called the floating type.

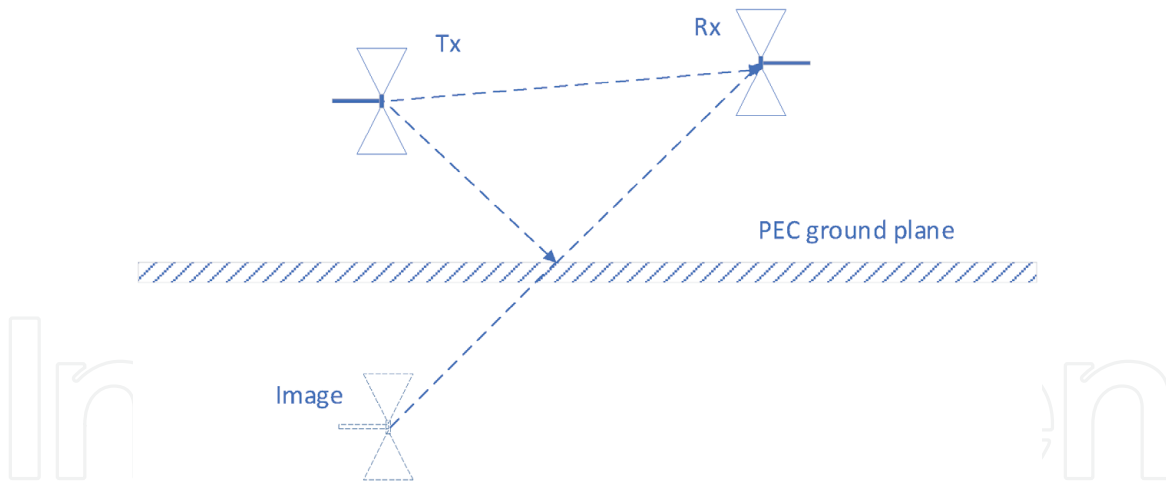


Figure 1.
 The theoretical model of an OATS—Half-space model.

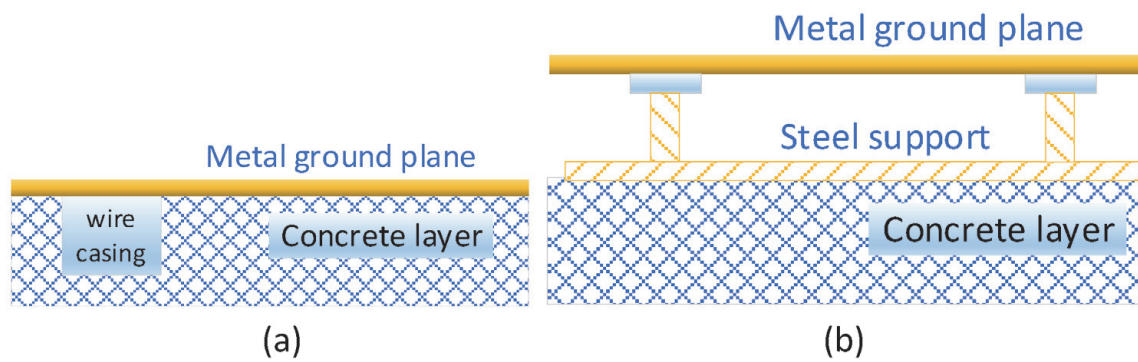


Figure 2.
 The structures of the ground plane. (a) Solid type and (b) floating type.

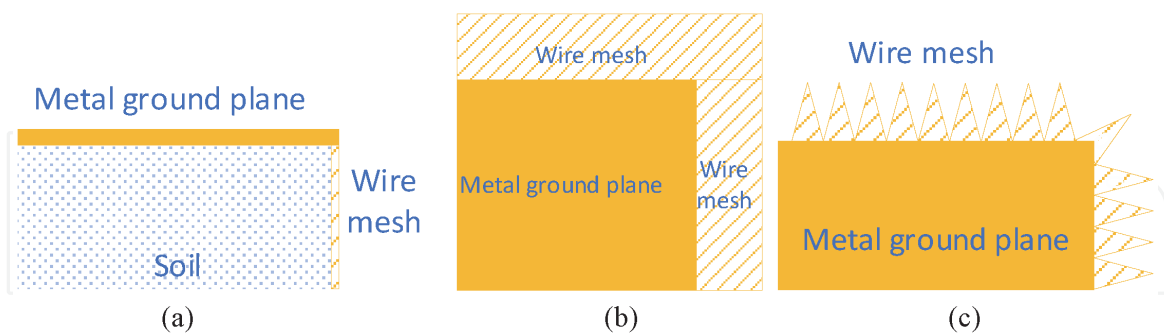


Figure 3.
 The design of stainless wire mesh (showing the corner of an OATS). (a) Inverted L-shape (vertical cut), (b) belt (bird view), and (c) triangular (bird view).

The impedance transition between the edge of the ground plane and the soil is also important. Usually, stainless wire mesh is designed for this purpose. **Figure 3** shows some typical designs for the stainless wire mesh. In (a), the wire mesh is mounted vertically down to the soil. In (b), a wire-mesh belt is mounted around the edge of the metal ground plane. In (c), the belt is replaced by some triangular wire mesh. Simulation shows design (c) agrees best with the theoretical mode in **Figure 1**, under the same ground plane size and wire mesh area.

Figure 4 shows the surface current induced. A pair of dipole antennas are resonated at 30 MHz and VP; the dipole antennas are separated by 20 m ($R = 20$ m)

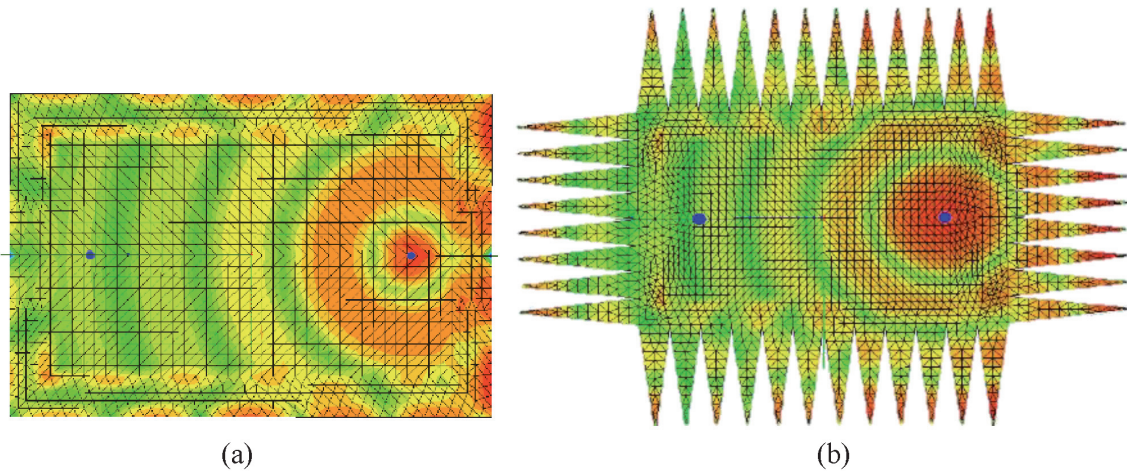


Figure 4.
The comparison of triangular wire mesh. (a) No wire mesh and (b) triangular wire mesh.

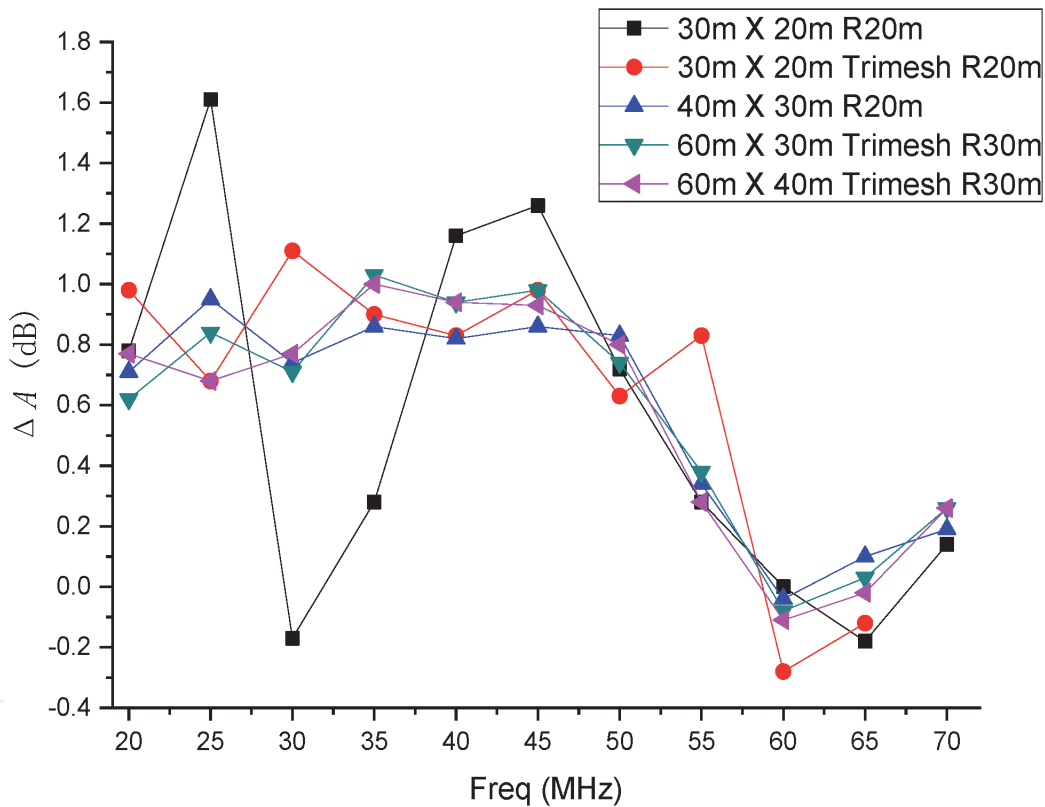


Figure 5.
The deviation of finite-size GP at VP ($R = 20\text{ m}$).

both the Tx and the Rx are 1.3 m above the perfect electric conductor (PEC) ground plane. The height of the isosceles triangles is 10 m, and the bottom width is 5 m. The inner area (25 m by 15 m) of the ground plane is simulated with physical optics (PO), while others are simulated with Method of Moment (MoM). The simulation model is set up in free space; in other words, no consideration is taken into account on the effect of the grounding of wire mesh into the soil. **Figure 4** shows that the surface current fluctuated rapidly near the edge of the ground plane or the tips of the mesh [7].

The deviation ΔA is shown in **Figure 5**. The means for the legends are shown below:

1. “30 m × 20 R20 m”: no wire mesh, as shown in **Figure 4(a)**, GP is 30 m by 20 m, both dipole antennas are separated by 20 m;
2. “30 m × 20 Trimesh R20 m”: triangular wire mesh as shown in **Figure 4(b)** is introduced based on ①; The meanings for other legends are similar.

As shown in [7], a GP of 30 m by 20 m is not qualified for measurements at R = 20 m, whose deviation is larger than 1.5 dB. However, it can be reduced to 1.2 dB at VP by introducing some triangular wire mesh shown in **Figure 4(b)**. If the GP is increased to 40 m by 30 m, the deviation is less than 1 dB. Less deviation at 30 m separation can be achieved by increasing the GP to 60 m by 40 m.

Further simulation shows that the triangular wire mesh is also effective for HP at R = 20 m, as shown in **Figure 6**.

The performance of a practical OATS should be as close as possible to the half-space model shown in **Figure 1**. The IEC standard CISPR 16–1-5:2014 provides a detailed method to validate this, which is briefly summarized as in Eq. (1).

$$\Delta A = |A_m - A_c| < T_{SIL} - \Delta A_m. \quad (1)$$

where ΔA is the absolute deviation of the OATS from an ideal OATS, in dB, at the specified frequency; A_m is the measured site insertion loss (SIL), in dB, between a pair of calculable dipole antennas; ΔA_m is the SIL measurement uncertainty ($k = 2$), in dB, A_c the calculated SIL, in dB; T_{SIL} is the allowed tolerance in SIL, in dB. For a calibration test site (CALTS), $T_{SIL} = 1.0$ dB at horizontal polarization (HP).

For a reference test site (REFTS), $T_{SIL} = 1.0$ dB at HP and $T_{SIL} = 1.5$ dB at vertical polarization (VP). **Table 1** lists some famous OATS in the world. Where CR stands for the control room (CR), some data are not available (N/A) due to the limited knowledge of the author.

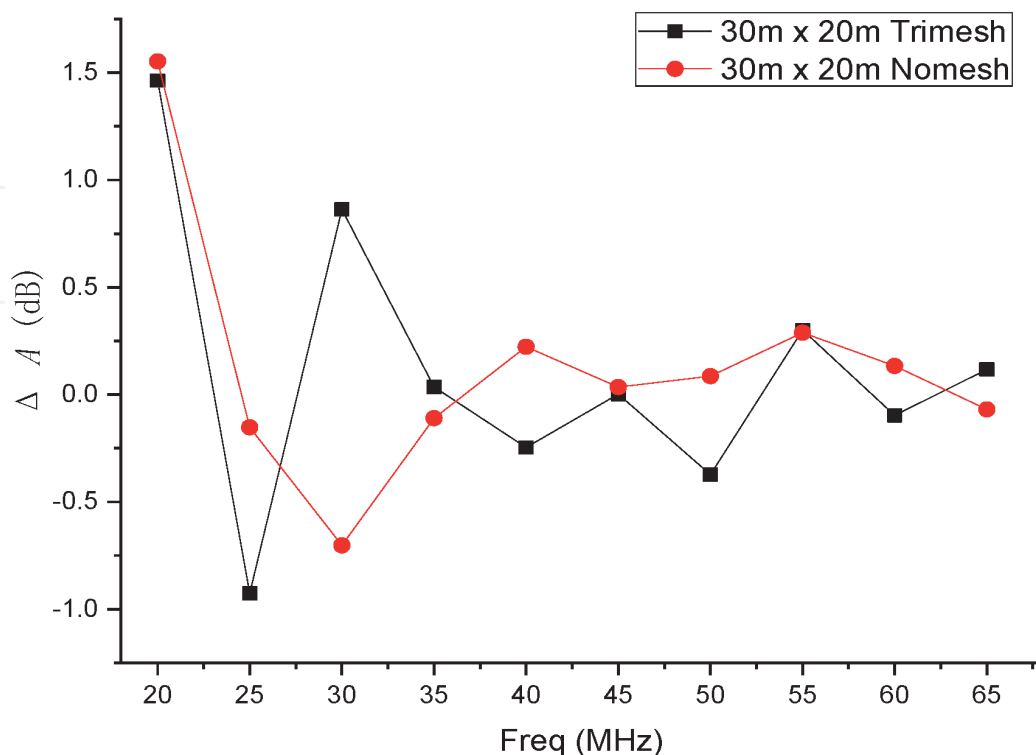


Figure 6.
 The deviation of finite-size GP at HP (R = 20 m).

Lab.	Dimensions		Structure	CR Locations	ΔA^*
	Metal GP	Stainless wire mesh			
NIM (China)	60 m x 40 m x 10 mm	10 m Triangular	Floating type	Under	0.26 dB (HP) 0.34 dB (VP)
NPL (UK)	60 m x 30 m x 8 mm	Inverted L-type	Solid type	Above GP, Wooden, 25 m far away	0.3 dB (HP)
NIST (USA)	60 m x 30 m x 8 mm	Triangular	Solid type	N/A	N/A
Liberty Lab. (USA)	60 m x 30 m x 8 mm	Rectangular 10 m width	Floating type	Half under	0.5 dB (HP)
ETS-LINDGREN (USA)	60 m x 30 m x 8 mm	Strip	Solid type	Under	N/A
NIMJ (Japan)	45 m x 30 m x 16 mm	Rectangular	Floating type	Above GP	N/A
KRISS (Korea)	30 m x 30 m x 2 mm	N/A	Solid type	N/A	N/A
CENAM (Mexico)	60 m x 30 m	N/A	N/A	N/A	0.5 (HP)
ARC (Austria)	20 m x 17 m	Rectangular 10 m width	Solid type	Under GP, with 50 cm roof above GP	N/A

**Due to the limited knowledge of the author, the data could be wrong. N/A, not available.*

Table 1.
Some high-performance OATS.

3. A case study for NIM OATS

Figure 7 shows a photo of NIM OATS taken in 2014. It is located in NIM's Changpin Campus. The white part is the reflective GP, and usually, there are a motorized mast and a manual mast for holding the antennas to be measured. The masts are made of low permittivity dielectric materials. The motor of the motorized mast is located under the metal GP to avoid unwanted reflections. Obviously, these setups will imitate the theoretical model shown in **Figure 1**.



Figure 7.
Photo of NIM OATS.

BTW, in this photo, there are two more masts on the upper right corner of the GP, which is for backup, and it would better be moved away. There is also a beautiful lake in the north of the OATS. Some sand cypress trees are planted around to keep the soil wet and as fences to prevent the entrance of unintentional persons and trucks.

The structure of the OATS is illustrated in **Figure 8**.

The whole system is designed carefully. The metal GP will suffer more than 80 degrees temperature variations seriously during four seasons in Beijing. In order to cope with this critical problem, the large metal GP is placed “freely” on the top 2501 pieces (41 by 61) of the ceramics plate. The metal GP can move freely in the horizontal plane but is kept fixed in the vertical direction. The ceramics plates are mounted on adjustable bolts, which are mounted on the steel frames. These steel frames are mounted on the box-layered concrete structure. The whole concrete structure is located on 138 pile foundations, which are over 20 m deep into the rock layer, to maintain a very stable foundation.

As shown in **Figure 8**, the equipment room (ER) is located under the bottom of antenna masts, which can make sure the shortest cable routing from antenna masts

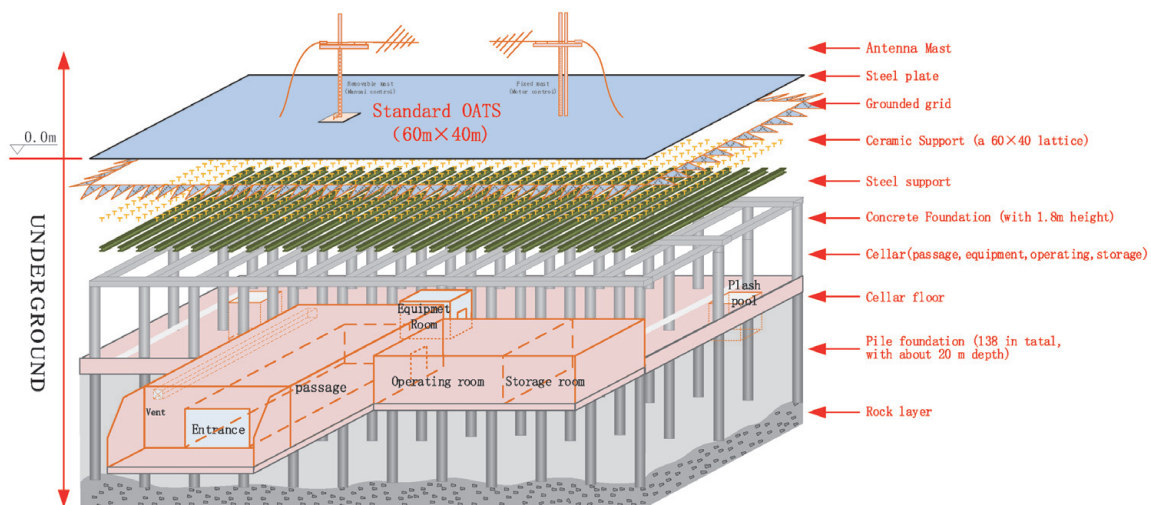


Figure 8.
The structure illustration of NIM OATS.

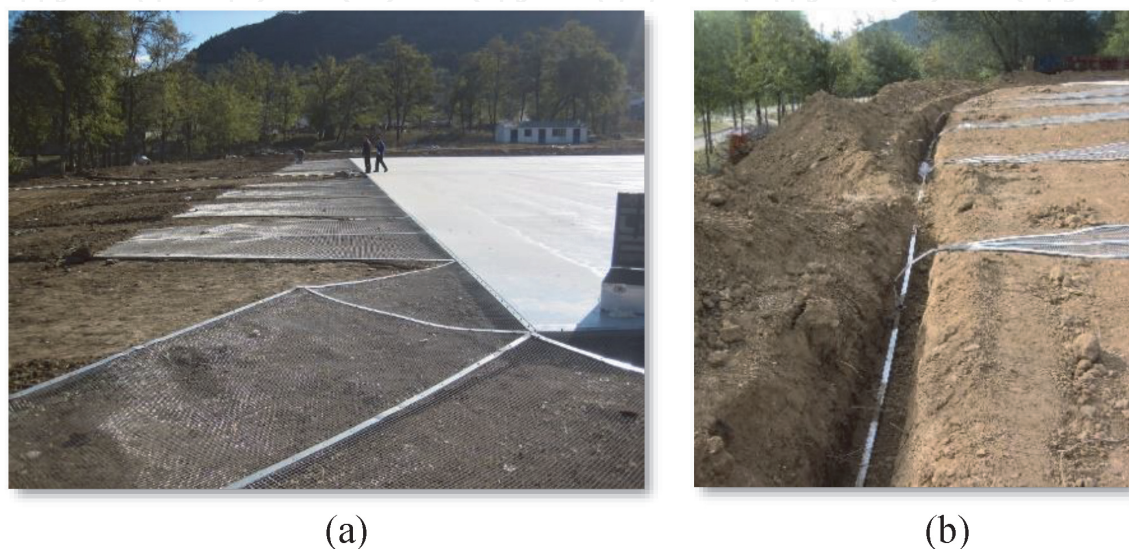


Figure 9.
The grounding of the triangular wire mesh. (a) Triangular wire mesh and (b) tip of the triangular wire mesh.

to the ER. The control room is located under the GP, but near the entrance, to make sure a short way for operators to make measurements.

The dimension of the GP and stainless triangular wire mesh are shown in **Figure 9**.

As shown in **Figures 4–6**, the triangular is very useful for reducing the reflections from the edge of the GP. **Figure 9(a)** is the photo for the stainless triangular wire mesh, and **Figure 9(b)** shows the tips of the triangular wire mesh connected each other and being grounded to the soil with resistance less than $1\ \Omega$.

Lots of precise “measurements” are carried out for this OATS. The deviation ΔA shown in Eq. (1) measured with a pair of calculable dipole antennas (CDAs) at 24 resonant frequencies is shown in **Figure 10** for HP and **Figure 11** for VP [7].

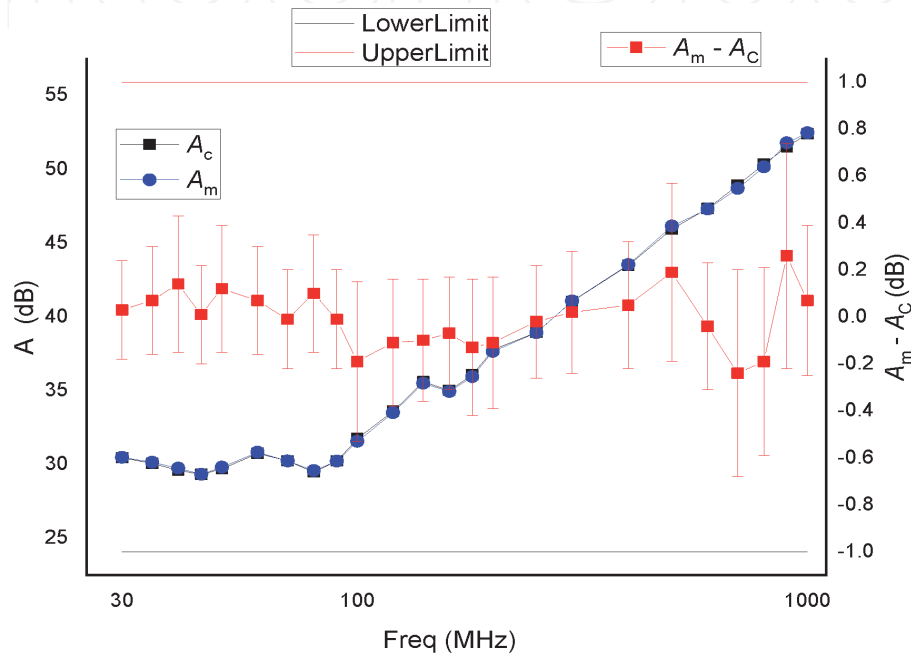


Figure 10.
The deviation of NIM's OATS at HP.

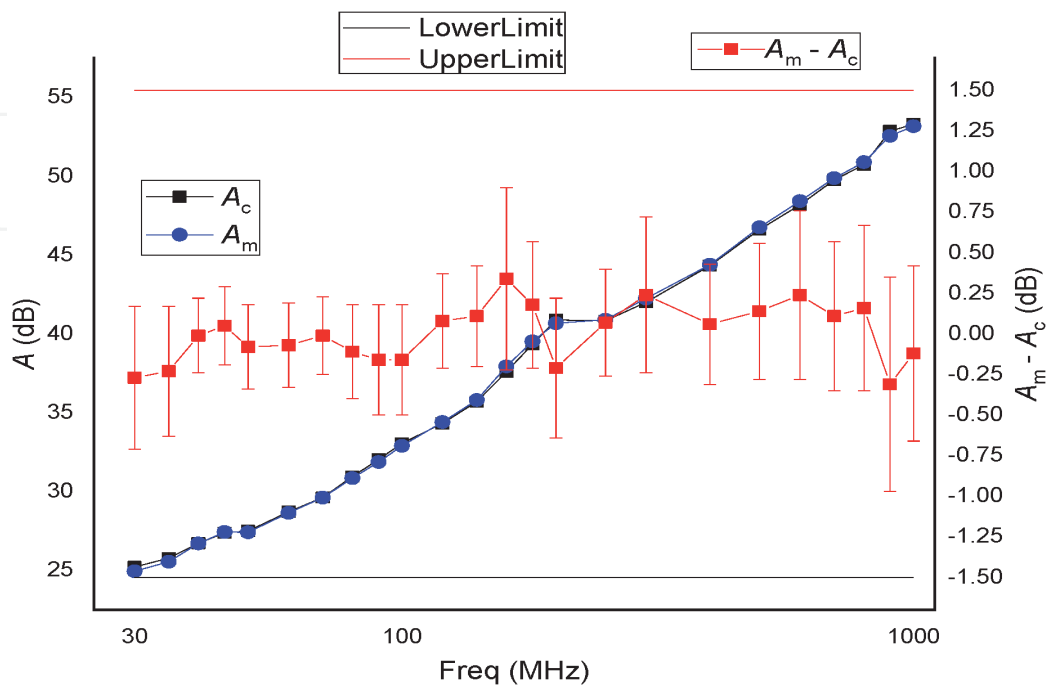


Figure 11.
The deviation of NIM's OATS at VP.

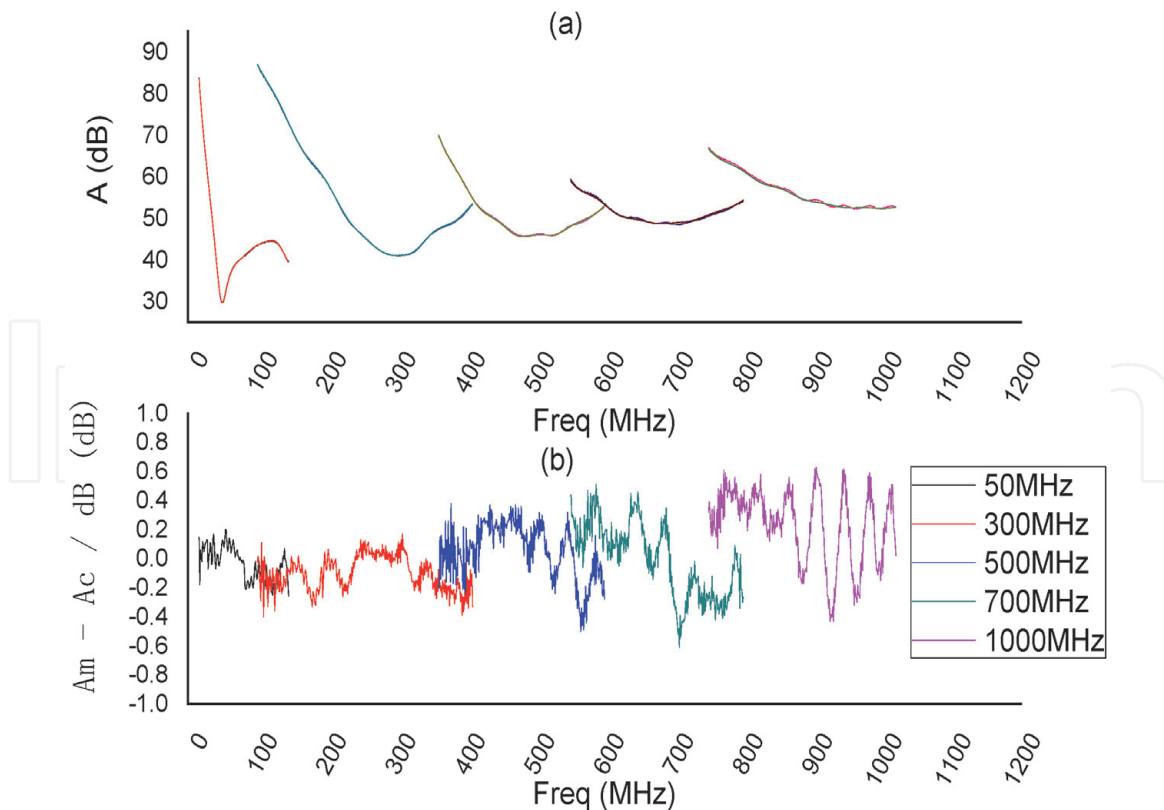


Figure 12. Deviation of NIM's OATS over sweeping frequencies, HP, $R = 10$ m. (a) the comparison of measured and calculated site insertion loss (A). (b) the difference of site insertion loss between measurements and calculations.

The deviation is less than 0.26 dB for HP and 0.34 dB for VP. Obviously, it meets the requirements for both CALTS and REFT, though the uncertainty ΔA_m is over-estimated. Thus, we can conclude that the performance of this OATS is wonderful.

In order to investigate the results at other frequencies, sweeping measurements between a pair of broadband calculable dipole antennas separated by 10 m and HP are shown in **Figure 12**. The difference between A_m and A_c are quite less at resonant frequencies, e.g., 50 MHz, 300 MHz, 500 MHz, 700 MHz, and 1000 MHz; however, it is larger at non-resonant frequencies.

4. Uncertainty evaluation of antenna factor F_a for biconical antennas with standard site method

The setup of the standard site method (SSM) is shown in **Figure 13**. The Rx is swept from 1 m to 4 m in height to get the minimum SIL (and this is defined as site attenuation-SA). The horizontal separation R between the center (reference locations) of both antennas is 10 m.

After measuring three SAs for three pairs of antennas (#1 vs. #2, #1 vs. #3, and #2 vs. #3), respectively, the free-space antenna factor F_{a_1} of antenna #1 can be calculated with Eq. (2) [5].

$$F_{a_1} = 10 \lg f_M - 24.46 + \frac{1}{2} [E_D^{\max} + A_{12} + A_{13} - A_{23}] + \Delta F_{DevFree-space} \quad (2)$$

Where f_M is the frequency in MHz; $A_{i,j}$ is the site attenuation between antenna # i and j , ($i = 1, 2, 3; j = 1, 2, 3; i \neq j$). E_D^{\max} can be calculated according to Eq. (3),

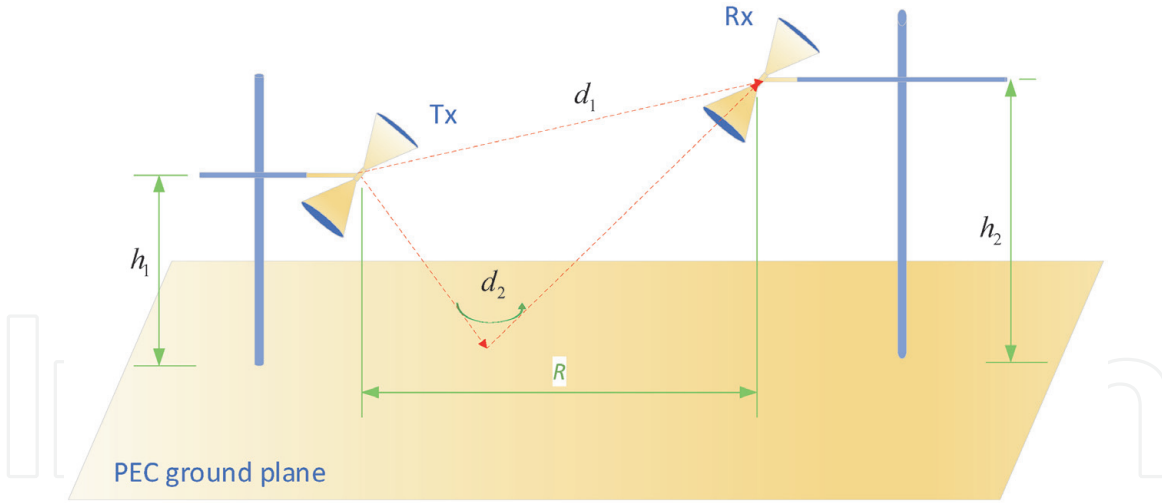


Figure 13.
The setup of the SSM.

$$E_D^{\max} = 20 \lg \left\{ \frac{\sqrt{49.2 [d_1^2 + d_2^2 + 2d_1d_2 \cos [\beta(d_2 - d_1)]]}^{1/2}}{d_1d_2} \Big|_{1 \leq h_2 \leq 4} \right\}. \quad (3)$$

Where

$$d_1 = [R^2 + (h_1 - h_2)^2]^{1/2}, \quad (4)$$

$$d_2 = [R^2 + (h_1 + h_2)^2]^{1/2}, \quad (5)$$

$$\beta = \frac{2\pi f_M}{300}. \quad (6)$$

where $\Delta F_{DevFree-space}$ is the correction factor, as shown in Table G.1 in [5]. The meanings for other symbols are shown in **Figure 13**.

It is very hard to deduce an analysis equation for measuring antenna factor. Usually, a hybrid model (both analytical and dark box model) is adopted, as shown in Eq. (7) as an example,

$$\begin{aligned} F_{a1SSM} = & 10 \lg f_M - 24.46 + \frac{1}{2} E_D^{\max} + \left[\frac{1}{2} A_{12} + \frac{1}{2} A_{13} - \frac{1}{2} A_{23} \right] + \frac{\sqrt{3}}{2} u(\delta A_{VNA}) \\ & + \frac{\sqrt{3}}{2} u(\delta A_{Impedance}) + \frac{\sqrt{3}}{2} u(\delta A_{Cable}) + \frac{\sqrt{3}}{2} u(\delta A_{Thru}) + \frac{\sqrt{3}}{2} u(\delta A_{AN}) \\ & + \frac{\sqrt{3}}{2} u(\delta A_{AntPosition}) + \frac{\sqrt{3}}{2} u(\delta A_{Site\&Mast}) + \frac{\sqrt{3}}{2} u(\delta A_{Repeat}) + \frac{\sqrt{3}}{2} u(\delta A_{Symetry}) \\ & + \frac{\sqrt{3}}{2} u(\delta A_{X-pol}) + \Delta F_{DevFree-space} \end{aligned} \quad (7)$$

The meaning of the other symbols is shown in **Table 2**. The evaluated standard uncertainty is shown in **Table 2**, too. The combined standard uncertainty can be calculated with Eq. (8), assuming the above uncertainty sources are independent.

$$\begin{aligned}
 u_c^2(F_{a1}) = & \left[\frac{\sqrt{3}}{2} u(\delta A_{VNA}) \right]^2 + \left[\frac{\sqrt{3}}{2} u(\delta A_{Impedance}) \right]^2 + \left[\frac{\sqrt{3}}{2} u(\delta A_{Cable}) \right]^2 \\
 & + \left[\frac{\sqrt{3}}{2} u(\delta A_{Thru}) \right]^2 + \left[\frac{\sqrt{3}}{2} u(\delta A_{AN}) \right]^2 + \left[\frac{\sqrt{3}}{2} u(\delta A_{AntPosition}) \right]^2 \\
 & + \left[\frac{\sqrt{3}}{2} u(\delta A_{Site\&Mast}) \right]^2 + \left[\frac{\sqrt{3}}{2} u(\delta A_{Repeat}) \right]^2 + \left[\frac{\sqrt{3}}{2} u(\delta A_{Symetry}) \right]^2 \\
 & + \left[\frac{\sqrt{3}}{2} u(\delta A_{X-pol}) \right]^2 + u^2(\Delta F_{DevFree-space})
 \end{aligned} \tag{8}$$

Relating the value in **Table 2**, there will be,

$$u_c = 0.68 \text{ dB} \tag{9}$$

The expanded uncertainty can be calculated with Eq. (4) by assuming a normal distribution since there are many numbers, and their values are similar.

No.	Symbol	Source of uncertainty or quantity (X_i)	Value (dB)	Probability	Divisor	Sensitivity	Standard uncertainty (u_i ; dB)
1	δA_{VNA}	Uncertainty from measuring S21 with VNA	0.25	Normal	2	$\frac{\sqrt{3}}{2}$	0.11
2	$\delta A_{Impedance}$	Impedance mismatch between transmit and receive antennas	0.28	U-shaped	$\sqrt{2}$	$\frac{\sqrt{3}}{2}$	0.17
3	δA_{Cable}	Cable loss variation due to temperature variation	0.2	Rectangular	$\sqrt{3}$	$\frac{\sqrt{3}}{2}$	0.10
4	δA_{Thru}	Uncertainty from through calibration	0.2	Rectangular	$\sqrt{3}$	$\frac{\sqrt{3}}{2}$	0.10
5	δA_{AN}	Ambient noise	0.1	Normal	2	$\frac{\sqrt{3}}{2}$	0.04
6	$\delta A_{AntPosition}$	Antenna positing error	0.26	U-shaped	$\sqrt{2}$	$\frac{\sqrt{3}}{2}$	0.16
7	$\delta A_{Site\&Mast}$	Imperfection of the OATS and masts	0.6	Rectangular	$\sqrt{3}$	$\frac{\sqrt{3}}{2}$	0.30
8	δA_{Repeat}	Repeatability of the measurement system	0.3	Normal	2	$\frac{\sqrt{3}}{2}$	0.13
9	$\delta A_{Symetry}$	Symmetry of the antenna under measurement	0.8	Rectangular	$\sqrt{3}$	$\frac{\sqrt{3}}{2}$	0.40
10	δA_{X-pol}	Cross-polarization	0	Rectangular	$\sqrt{3}$	$\frac{\sqrt{3}}{2}$	0.00
11	$\Delta F_{DevFree-space}$	Deviation from the free-space antenna factor	0.4	Rectangular	$\sqrt{3}$	1	0.23
12	Combined standard uncertainty, u_c						0.68
13	Expanded uncertainty, U ($k = 2$)						1.4

Table 2.
 Measurement uncertainty budget for F_a of a biconical antenna with standard site method.

$$U = ku_c \quad (10)$$

Taking $k \approx 2$, there will be

$$U = 1.4 \text{ dB } (k = 2) \quad (11)$$

This is the expanded uncertainty in measuring the free-space antenna factor of a biconical antenna with the standard site method, as shown in **Table 2**.

5. Conclusion

Key technologies on the design, construction and validation of a high-performance OATS have been provided, based on the author's many years of experience. Some famous OATS in the world regarding their structure, the dimensions of the ground plane (GP), the location of the control room, and performance have been summarized. A detailed case study is provided on NIM's high-performance OATS. A measurement uncertainty example has been provided in measuring the free-space antenna factor of biconical antennas.

Acknowledgements

Dr. Alexander KRIZ and Dr. Katsumi Fujii provide many details on their OATS. There are many persons involved in the design, construction, and validation of NIM's OATS. Special acknowledgments are due to TDK, Mr. Gao X. X., Dr. Cui X. H., Dr. Song Z. F., Mr. Hong L., and Ban H.

Conflict of interest

The author declares no conflict of interest.

Abbreviations

	Full name	Symbol
OATS	open-area test site	/
CALTS	calibration test site	/
REFTS	reference test site	/
GP	ground plane	/
PEC	perfect electric conductor	/
CR	control room	/
ER	equipment room	/
CDA	calculable dipole antenna	/
MoM	Method of Moments	/
NIM	National Institute of Metrology	/
SA	site attenuation	/
NSA	normalized site attenuation	/
HP	horizontal polarization	/
VP	vertical polarization	/
SIL	site insertion loss	/
/	calculated site insertion loss	A_c
/	measured site insertion loss	A_m
/	free-space antenna factor	F_a

IntechOpen

IntechOpen

Author details

Donglin Meng
National Institute of Metrology, Beijing, China

*Address all correspondence to: mengdl@nim.ac.cn

IntechOpen

© 2021 The Author(s). Licensee IntechOpen. This chapter is distributed under the terms of the Creative Commons Attribution License (<http://creativecommons.org/licenses/by/3.0>), which permits unrestricted use, distribution, and reproduction in any medium, provided the original work is properly cited. 

References

- [1] CISPR 16-1-6, Edition 1.1 2017-01, Specification for radio disturbance and immunity measuring apparatus and methods – Part 1-6: Radio disturbance and immunity measuring apparatus – EMC antenna calibration. EMC Technologies (MAPE), DOI: 10.1109/MAPE.2015.7510308, 2015.
- [2] CISPR 16-1-5:2014+AMD1:2016 CSV, Specification for radio disturbance and immunity measuring apparatus and methods – Part 1-5: Radio disturbance and immunity measuring apparatus – Antenna calibration sites and reference test sites for 5 MHz to 18 GHz.
- [3] CISPR 16-1-4, Edition 4.0 2019-01, Specification for radio disturbance and immunity measuring apparatus and methods – Part 1-4: Radio disturbance and immunity measuring apparatus – Antennas and test sites for radiated disturbance measurements.
- [4] Meng D. L. “A fast way to accurately calibrate tunable dipole antennas at VHF,” *IEEE Transactions on Electromagnetic Compatibility* 60(1): 10. 2018.
- [5] ANSI C63.4a-2017 (Amendment to ANSI C63.4-2014), American National Standard for Methods of Measurement of Radio-Noise Emissions from Low-Voltage Electrical and Electronic Equipment in the Range of 9 kHz to 40 GHz.
- [6] Martin Alexander, Martin Salter, Benjamin Loader, and David Knight, “Broadband calculable dipole reference antennas,” *IEEE Transactions on Electromagnetic Compatibility*, 44(1): 45-58. PII: S 0018-9375(02)01461-8, 2002.
- [7] D. L. Meng., X. Liu, and D. B. Li, “Research on unwanted reflections in an OATS for precise omni antenna measurement,” *Proceedings of the IEEE 6th International Symposium on Microwave, Antenna, Propagation, and*